JOURNAL of the MEXICAN CHEMICAL SOCIETY

https://www.jmcs.org.mx/

Review

Open Access

J. Mex. Chem. Soc. **2026**, *70(1):e2583*

Received November 12th, 2025
Accepted December 22nd, 2025

http://dx.doi.org/10.29356/jmcs.v70i1.2583
e-location ID: 2583

Keywords:
Hemicyanine dyes; intramolecular charge transfer; solvatochromism; near-infrared fluorescence; bioimaging; theranostics

Palabras clave:
Hemicianinas; transferencia de carga intramolecular; solvatocromismo; fluorescencia de infrarrojo cercano; bioimagen; teranóstica

***Corresponding author:**
Juan F. Tamez-Fernández
email: juan.tamezfrn@uanl.edu.mx
Pablo Rivera-Fuentes
email: pablo.riverafuentes@uzh.ch

©2026, edited and distributed by Sociedad Química de México

ISSN-e 2594-0317

Hemicyanine Compounds as Versatile Tools in Chemical Biology and Medicinal Chemistry

Juan F. Tamez-Fernández[1*], Pablo Rivera-Fuentes[2*]

[1]Universidad Autónoma de Nuevo León, Facultad de Medicina, Departamento de Química Analítica, Monterrey, Nuevo León, México.
[2]Department of Chemistry, University of Zurich, Zurich, Switzerland.

Abstract. Hemicyanine dyes comprise a versatile family of donor–π–acceptor (D–π–A) chromophores, characterized by tunable intramolecular charge-transfer transitions that yield strong visible-to-near-infrared absorption and emission. Their modular scaffolds, high molar absorptivity, and environment-responsive photophysics have made them indispensable in fluorescence imaging, photoacoustic sensing, and the development of theranostic probes. Over the past two decades, structural refinements, including the incorporation of heterocyclic donors, polymethine elongation, and acceptor substitution, have expanded the spectral range into the NIR-II region, improved photostability, and enabled ratiometric and activatable response mechanisms. In this review, we summarize fundamental photophysical principles, structural determinants of optical behavior, and representative examples of hemicyanine derivatives that bridge chemistry and biology.

Resumen. Los compuestos hemicianina constituyen una familia versátil de cromóforos donador–π–aceptor (D–π–A), caracterizados por transiciones de transferencia de carga intramolecular sintonizables que dan lugar a una intensa absorción y emisión en la región visible–infrarrojo cercano. Sus estructuras modulares, la alta absorbancia molar y una fotofísica sensible al entorno los han convertido en herramientas indispensables en bioimagen por fluorescencia, detección fotoacústica y desarrollo de sondas teranósticas. Durante las últimas dos décadas, las optimizaciones estructurales, incluida la incorporación de

©2026, Sociedad Química de México. Authors published within this journal retain copyright and grant the journal right of first publication with the work simultaneously licensed under a Creative Commons Attribution License that enables reusers to distribute, remix, adapt, and build upon the material in any medium or format for noncommercial purposes only, and only so long as attribution is given to the creator.

J. Mex. Chem. Soc. **2026**, *70(1):e2583*
Regular Issue
©2026, Sociedad Química de México
ISSN-e 2594-0317

donadores heterocíclicos, la elongación del puente polimetínico y la sustitución en el aceptor, han extendido el intervalo espectral hasta la región NIR-II, mejorado la fotostabilidad y permitido mecanismos de respuesta ratiométrica y activable. En esta contribución se resumen los principios fotofísicos fundamentales, los determinantes estructurales del comportamiento óptico y ejemplos representativos de derivados de hemicianinas que conectan la química con la biología.

Introduction

Cyanine and hemicyanine chromophores have served as foundational scaffolds for organic photonics and bioimaging since the early twentieth century.[1,2] Hemicyanines, characterized by a donor–π–acceptor (D–π–A, Fig. 1 conjugated motif that is usually capped with a cationic heterocycle, exhibit pronounced intramolecular charge-transfer transitions that yield intense absorption and fluorescence across the visible and near-infrared (NIR) spectral window.[3–5] Their asymmetry produces strong dipole moments and environment-dependent emission, rendering them exceptionally responsive to variations in polarity, viscosity, and pH,[5–8] among other stimuli.

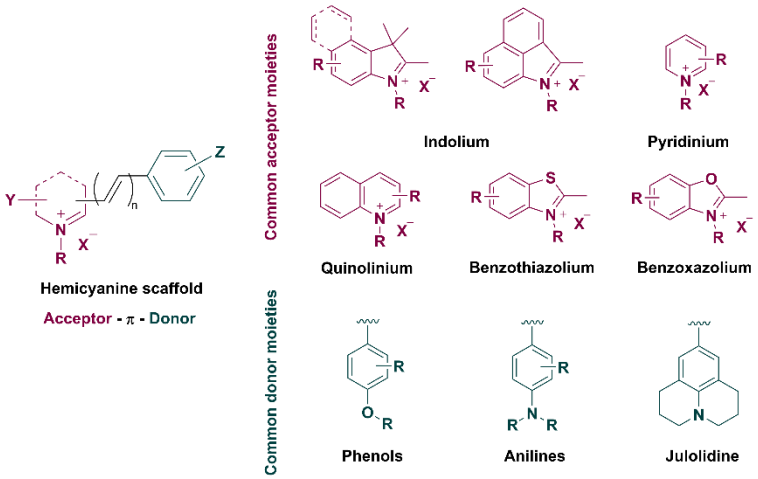

Fig. 1. Chemical structure of hemicyanine components. Structures of common donor and acceptor moieties.

During the past two decades, these dyes have evolved from fundamental spectroscopic curiosities to indispensable molecular tools in chemical biology and medicinal chemistry. Early work focused on understanding solvent effects, aggregation phenomena, and electronic coupling within polymethine frameworks.[1,7–12] Subsequent synthetic diversification introduced a rich variety of heterocycles such as indolium, benzothiazolium, quinolinium, and others, coupled through polymethine linkers to electron-donating moieties such as anilines, phenols, or julolidine derivatives (Fig. 1).[1,2,5] This modularity facilitated systematic modulation of absorption maxima (λabs), fluorescence wavelengths (λem), and quantum yields (Φf).

In biomedical contexts, hemicyanine derivatives offer unique advantages over traditional fluorophores. Their NIR absorption and emission minimize background autofluorescence, improve tissue penetration, and enable deep-tissue visualization of biological processes.[3] Chemical modification, introducing reactive triggers, targeting ligands, or zwitterionic substituents, has converted simple dyes into activatable or environment-specific probes.[3,4] Recent developments have expanded emission further into the second NIR window (NIR-II, also known as shortwave infrared—SWIR—region: 900−1700 nm), affording improved spatial resolution and signal-to-noise ratios for *in vivo* imaging.[13,14] This review highlights the structural, photophysical, and mechanistic insights of hemicyanine compounds and surveys their translational impact as molecular sensors and therapeutic agents.

http://dx.doi.org/10.29356/jmcs.v70i1.2583

J. Mex. Chem. Soc. **2026**, *70(1):e2583*
Regular Issue
©2026, Sociedad Química de México
ISSN-e 2594-0317

Structural and photophysical features

The photophysical diversity of hemicyanine dyes arises from the delicate balance of their electronic structure and local environment. Rational engineering of donor, acceptor, and bridge components enables continuous spectral tuning from visible to SWIR regions while maintaining stability and brightness. Understanding these fundamental photophysical characteristics provides the mechanistic rationale for the chemical biology and medicinal chemistry applications of hemicyanine dyes.

General structure and substituent effects

Hemicyanine dyes are typically synthesized by condensing an electron-rich aromatic aldehyde (e.g., aniline, indoline, or julolidine derivatives) with a quaternary heterocyclic salt such as indolium, quinolinium, or benzothiazolium. This Knoevenagel or aldol-type condensation forms a conjugated polymethine bridge characteristic of the hemicyanine scaffold (Scheme 1**(A)**).[1,2,4,5] Recent advances have refined this traditional synthetic route, exemplified by the development of silicon-substituted analogues prepared via cross-coupling followed by Knoevenagel condensation (Scheme 1**(B)**), affording high yields and improved photostability.[15] Other strategies consist of degrading traditional cyanine dyes to create novel hemicyanine fluorophore structures (Scheme 1**(C)**).[5,13,16]

Tuning donor and acceptor sites provides spectral control. Strong donors (julolidine, dialkylamino) increase electron density, while strong acceptors (indolium, quinolinium, benzothiazolium) intensify intramolecular charge transfer (ICT).[1,3,5] Heteroatom substitutions (Si, P, S) and rigid linkers extend conjugation into the NIR-II region.[3,5,14,15,17]

Optical properties follow predictable D–A modulation trends: stronger donors raise the HOMO, and stronger acceptors lower the LUMO, narrowing the gap and red-shifting absorption.[14,18,19] Conversely, electron-withdrawing substituents (cyano, nitro, sulfonate) stabilize excited states, favoring photoacoustic signal generation.[18,20]

Hybrid architectures such as xanthene–, BODIPY–, rhodol–, naphthalimide–, and coumarin–hemicyanine fusions combine strong fluorescence with red-shifted emission, balancing radiative and non-radiative decay pathways (Fig. 2).[3,6,14,16,21–24] Extending the polymethine chain shifts absorption from the visible to >850 nm, but extending this bridge comes at the cost of increased susceptibility to photooxidation.[13,14,17,21,25] Stabilization strategies include bridge cyclization and heteroatom incorporation to limit torsion.[13,14,17,21,25]

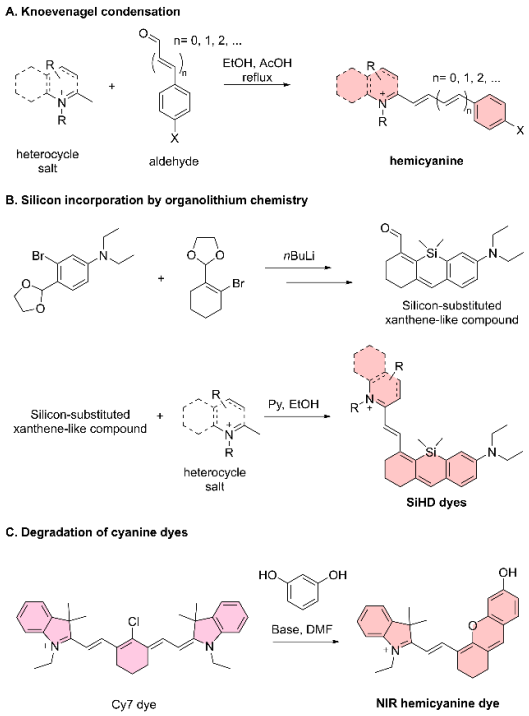

Scheme 1. Synthetic approaches for hemicyanine dye formation.

http://dx.doi.org/10.29356/jmcs.v70i1.2583

J. Mex. Chem. Soc. **2026**, *70(1):e2583*
Regular Issue
©2026, Sociedad Química de México
ISSN-e 2594-0317

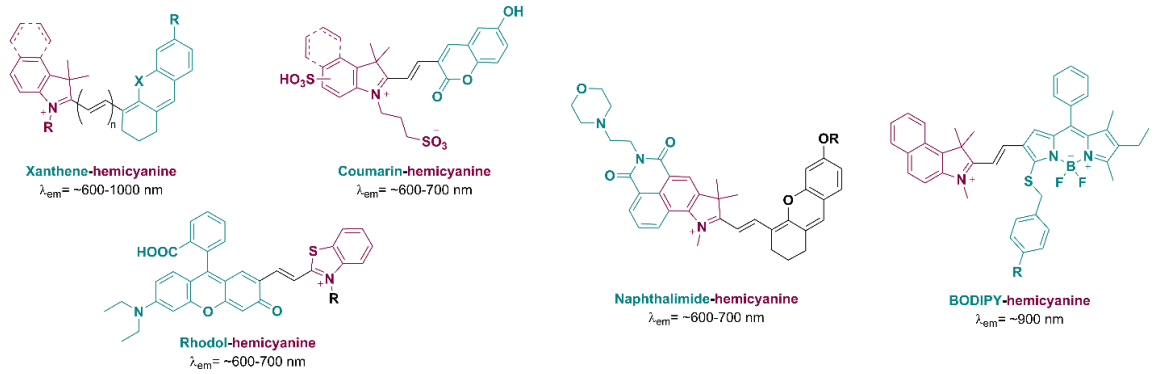

Fig. 2. Representative hemicyanine hybrid scaffolds and their approximate emission wavelengths

ICT and Solvatochromism

ICT describes the photoinduced migration of an electron from a donor to an acceptor moiety within a single molecule.[26] The optical behavior of hemicyanine dyes is largely governed by this donor–acceptor interaction: upon excitation, electron density shifts toward the acceptor, generating a highly polar excited state. [1,6,25,27] The photophysical properties of hemicyanines are therefore intrinsically environment-dependent, with solvent polarity, viscosity, and local dielectric effects collectively modulating ICT efficiency and fluorescence output.[28]

Stabilization of the charge-separated excited state by polar solvents results in positive solvatochromism, manifested as red-shifted emission and shortened fluorescence lifetimes in high-dielectric media.[1,8,28] Additionally, photoexcitation can induce rotation around the single bond connecting the donor and acceptor, producing a twisted ICT (TICT) state.[6,28,29] This conformational change disrupts the push–pull electronic equilibrium, diminishing fluorescence intensity. In low-viscosity environments, free molecular rotation favors non-radiative decay and weak emission, whereas in viscous media, restricted rotation suppresses TICT formation and enhances fluorescence.[28]

The extent of solvatochromism and TICT formation depends strongly on the molecular architecture of the dye, the nature of its chromophore, and the physicochemical properties of the surrounding medium. [28] Quantitative assessment of these effects is typically achieved by comparing ground- and excited-state dipole moments using Lippert–Mataga or McRae equations, which relate solvent-dependent spectral shifts to polarity parameters.[28]

Red-shifted photophysical properties

Strategic molecular engineering enables systematic extension of hemicyanine absorption and emission toward longer wavelengths. Approaches include: (i) elongation of the polymethine chain to increase conjugation length; (ii) introduction of heavy-atom or heteroatom donors to enhance π-delocalization; (iii) replacement of classical heterocyclic acceptors with benz[e]indolium, benzoimidazolium, or phosphinate-based units; and (iv) donor rigidification to suppress rotational relaxation.[14,15,17,21] These modifications have yielded dyes with emission maxima reaching 1000–1100 nm (NIR-II), suitable for deep-tissue imaging and photoacoustic detection.[14,20,30]

Relevance of these properties to biological environments

The distinctive photophysical and structural tunability of hemicyanine dyes directly underpins their versatility in biological systems. Their environment-sensitive solvatochromism and ICT behavior enable real-time visualization of microenvironmental polarity, viscosity, and pH within living cells. Extended conjugation and red-shifted absorption enhance tissue penetration and minimize autofluorescence, essential for deep-tissue and *in vivo* imaging. Meanwhile, improved photostability, reduced aggregation, and modular bioconjugation capacity allow hemicyanines to function as robust platforms for targeted imaging, sensing, and phototherapeutic applications in complex biological environments.

http://dx.doi.org/10.29356/jmcs.v70i1.2583

J. Mex. Chem. Soc. **2026**, *70(1):e2583*
Regular Issue
©2026, Sociedad Química de México
ISSN-e 2594-0317

Microscopy techniques that leverage hemicyanine dyes

The photophysical robustness of hemicyanine scaffolds supports a broad array of imaging modalities. Conventional confocal microscopy benefits from its high molar absorptivity and NIR fluorescence, minimizing photodamage and autofluorescence. [3,5,31] Two-photon excitation (700–900 nm) further enables deep-tissue optical sectioning with minimal scattering. Hemicyanine derivatives optimized for large two-photon cross-sections provide enhanced signal intensity in live-cell and intravital microscopy. [32] Recent developments of NIR hemicyanine dyes have leveraged hemicyanine scaffolds for their use as non-invasive contrast generation to apply in NIR fluorescence and photoacoustic imaging. [3,20,33,34]

Chemical biology applications

Hemicyanine-based fluorophores have emerged as powerful platforms for designing responsive probes capable of visualizing key biochemical parameters, including polarity, pH, reactive oxygen and nitrogen species (ROS/RNS), viscosity, and metal ions. Their high molar absorptivity, large Stokes shifts, and tunable ICT characteristics make them particularly well-suited for signal modulation in complex biological environments. [30]

Organelle targeting

Targeted imaging of intracellular organelles such as mitochondria and lysosomes has benefited greatly from the intrinsic cationic and lipophilic nature of hemicyanine dyes, which promote efficient membrane permeation and organelle accumulation. Fig. 3 summarizes representative structures and key features of these probes.

Recent developments in benzoindocyanine-derived hemicyanine probes underscore their versatility as mitochondria-targeted dual-function systems, integrating organelle imaging with enzyme or analyte responsiveness. A representative example, probe **1**, incorporates a 4-nitrobenzyl quencher to enable enzyme-activatable detection of nitroreductase while providing high-contrast mitochondrial fluorescence in live HeLa and A549 cells.[35] Similarly, probe **2** acts as a dual-response mitochondrial marker, capable of detecting both hypochlorous acid and sulfur dioxide, thereby enabling real-time visualization of oxidative stress under heat-shock conditions. [36] Furthermore, a series of dual-cationic hemicyanines (**3**–**5**) exhibits multimodal performance, combining selective bisulfite sensing and dual-channel mitochondrial imaging, with probe **5** additionally demonstrating photodynamic and photothermal activity. [37] Collectively, these examples highlight the adaptability of hemicyanine scaffolds for integrated sensing, subcellular targeting, and theragnostic applications, guided by emerging structure–activity relationships.

Complementary efforts have yielded benzothiazolium-based hemicyanine probes (**6**–**9**) designed as mitochondria-targeted viscosity sensors operating through the TICT mechanism. Among them, probe **8** exhibited outstanding mitochondrial selectivity and a 22-fold fluorescence enhancement with increasing viscosity, demonstrating its utility for mapping intracellular viscosity. [28]

In addition, pH-activatable NIR hemicyanine photosensitizer **10** was engineered as a mitochondria-targeted phototherapeutic, selectively activated in acidic tumor microenvironments to generate singlet oxygen under 660 nm irradiation, enabling fluorescence-guided photodynamic ablation of tumor cells with minimal off-target damage. [38]

For lysosomal imaging, a series of naphthalimide–hemicyanine hybrid probes (**11** and **12**) were developed as lysosome-targeted, dual-activatable fluorescent sensors, combining pH and viscosity responsiveness to achieve high-contrast NIR imaging. Notably, probe **11** exhibited exceptional lysosomal selectivity and sensitivity, allowing real-time visualization of microenvironmental changes and *in situ* diagnosis of acute gastritis. [6]

http://dx.doi.org/10.29356/jmcs.v70i1.2583

J. Mex. Chem. Soc. **2026**, *70(1):e2583*
Regular Issue
©2026, Sociedad Química de México
ISSN-e 2594-0317

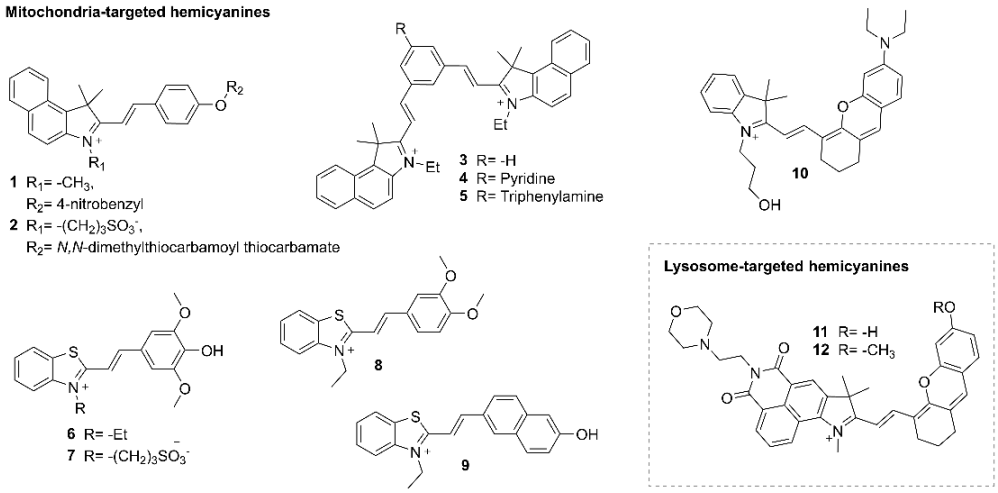

Fig. 3. Mitochondria- and lysosome-targeted hemicyanine probes.

Probes to sense ROS

Hydrogen peroxide (H_2O_2), a central ROS involved in redox signaling and oxidative stress, plays a pivotal role in maintaining cellular homeostasis and mediating pathological processes. [39] Advances in NIR hemicyanine probes have yielded highly sensitive and selective tools for detecting H_2O_2 in living systems. Two hemicyanine-based fluorescent probes incorporating a 4-nitro-α-ketoamide reactive switch (**13** and **14**) exhibited rapid, specific, and water-soluble fluorescence activation upon H_2O_2 recognition, enabling real-time imaging of endogenous and exogenous species in cells and animal models. [39,40] Probe **15** enabled visualization of autophagy-associated H_2O_2 generation, [41] while probes **16**–**18** achieved ultralow detection limits through boronate ester oxidation mechanisms. [16,42,43] Expanding the scaffold diversity, a benzothiazole-based hemicyanine probe **19** demonstrated a remarkable 284-fold fluorescence enhancement upon H_2O_2 activation, exemplifying the adaptability of this dye class for analyte sensing. [44]

Building on these strategies, hemicyanine fluorophores have also been adapted for the detection of hypochlorous acid (HClO), another biologically relevant ROS central to immune regulation and inflammation. [45] Probe **2** allowed hypochlorous acid sensing, enabling real-time visualization of oxidative stress under heat shock. [36] Ultrafast probes **20** and **21** exhibited nanomolar sensitivity and enabled real-time visualization of endogenous HClO dynamics during infection and inflammation, [45,46] while the refined probe **22** offered improved selectivity and biocompatibility for imaging oxidative stress in live cells and animal models. [47]

Superoxide ($O_2^{\bullet-}$), a primary ROS linked to oxidative damage and disease progression, has likewise been targeted by NIR hemicyanine probes. [48] The turn-on probe **23**, featuring a phosphinate recognition unit, enabled ultrasensitive (limit of detection—LOD = 10 nM), [48] biocompatible imaging of $O_2^{\bullet-}$ in zebrafish, mouse, and liver tissue. Complementarily, the dual-channel probe **24** allowed simultaneous detection of $O_2^{\bullet-}$ and peroxynitrite ($ONOO^-$) through orthogonal NIR and two-photon fluorescence pathways, facilitating dynamic visualization of reactive species interplay during drug-induced liver injury *in vitro* and *in vivo*.[49] Peroxynitrite is a potent RNS produced from nitric oxide and superoxide, and it plays a major role in oxidative inflammation and cellular damage. [50] The dual-modal NIR fluorescence and photoacoustic probe **25**, featuring a trifluoromethyl ketone-caged hemicyanine core, achieved nanomolar sensitivity and real-time $ONOO^-$ imaging in tumor-bearing mice. [50] Complementary ratiometric probes **26**–**28** [51] and the nanoliposome-encapsulated probe **29** [52] enabled selective mitochondrial $ONOO^-$ sensing and visualization of LPS-induced oxidative stress with large emission shifts and excellent biocompatibility, advancing the capability for subcellular nitrosative stress monitoring.

Additionally, benzoindocyanine-derived probe **30** employing a diphenylphosphinate-masked design demonstrated exceptional mitochondrial selectivity, an ultra-low detection limit (48 nM), and a 68-fold fluorescence enhancement upon $ONOO^-$ activation, effectively tracking dynamic $ONOO^-$ fluctuations in living

J. Mex. Chem. Soc. **2026**, *70(1):e2583*
Regular Issue
©2026, Sociedad Química de México
ISSN-e 2594-0317

cells and inflammatory zebrafish models. [53] The representative chemical structures and design principles of these ROS-responsive hemicyanine probes are summarized in Fig. 4.

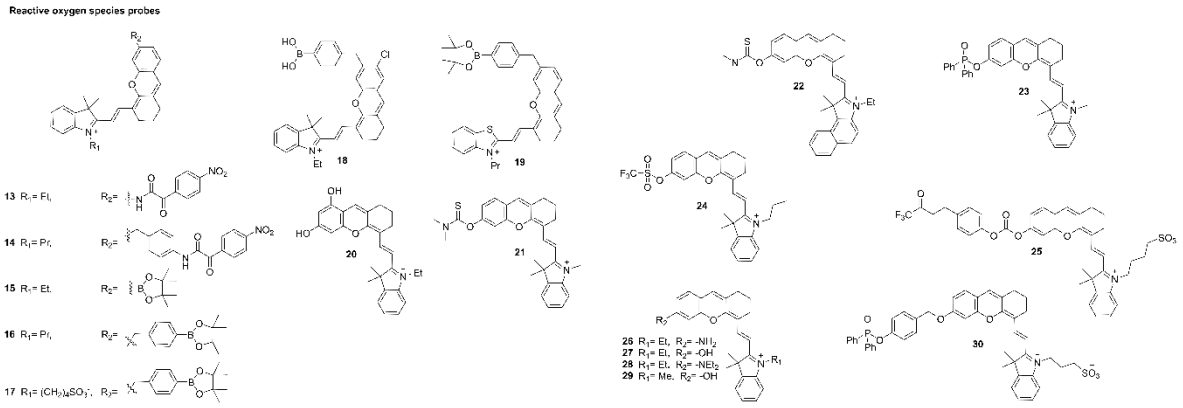

Fig. 4. Hemicyanine-based sensors of ROS.

Probes for Reactive Sulfur Species (RSS)

Hydrogen sulfide (H_2S), the third recognized endogenous gasotransmitter after nitric oxide and carbon monoxide, plays critical roles in neuromodulation, vascular regulation, and inflammation. [54,55] Consequently, real-time and selective monitoring of H_2S is essential to elucidate its physiological and pathological functions.[54,55] The hemicyanine scaffold has emerged as a versatile platform for designing NIR fluorescent probes with high sensitivity, selectivity, and excellent *in vivo* biocompatibility for H_2S detection.

The NIR-HS probe **31** enabled sensitive visualization of both exogenous and endogenous H_2S in living cells and mice, including cystathionine β-synthase overexpression models.[54] The Cy-PBA probe **32** achieved ultralow detection limits (21 nM) and rapid response times (<1.5 min), providing reliable tracking of H_2S dynamics across various biological contexts.[56] The ratiometric probe **33**, incorporating a triflate-reactive site, further improved analytical precision by combining nanomolar sensitivity (7 nM) with dual fluorescence and colorimetric outputs validated in cellular and zebrafish models.[55] In parallel, azide-based probes **34**[57] and **35**[58] exploited self-immolative and reduction-triggered activation mechanisms to achieve submicromolar detection limits and enable visualization of both endogenous H_2S generation and prodrug-derived release *in vitro* and *in vivo*. Finally, the sulfur-substituted probe **36** offered enhanced emission efficiency and fast turn-on response, enabling the first *in vivo* imaging of H_2S dynamics in an acute lung injury model.[59] Collectively, these probes illustrate the structural tunability and biological applicability of hemicyanine fluorophores for probing H_2S-mediated signaling pathways.

Beyond gaseous sulfur species, small-molecule thiols such as cysteine (Cys), homocysteine (Hcy), and glutathione (GSH) are key regulators of redox homeostasis and cellular metabolism.[60] Hemicyanine-based NIR probes have been extensively developed for their sensitive and selective visualization in complex biological environments. The turn-on probe **37**, based on a conjugate addition–cyclization reaction, displayed exceptional Cys selectivity with ultrafast kinetics and low detection limits suitable for live-cell and serum assays.[60] Similarly, the water-soluble probe **38**[61] achieved efficient discrimination of Cys from Hcy and GSH, while the mitochondria-targeted probe **39**[62] enabled precise imaging of endogenous mitochondrial Cys *in vitro* and *in vivo*. A related Cys-activatable system **40** offered rapid colorimetric and NIR fluorescence enhancement, facilitating Cys detection in both live cells and biological fluids.[63]

Progressing toward multifunctional systems, probe **41**[64] combined tumor-selective fluorescence activation with synergistic photodynamic and photothermal activity, and probe **42**[65] incorporated an isothiocyanate-triggered self-immolative mechanism for dual Cys sensing and H_2S release. Expanding to broader RSS detection, probe **43**[66] enabled nanomolar-level biothiol sensing across mammalian and bacterial systems, while the dual-modal probe **44**[67] exploited tumor-associated GSH overexpression for combined NIR fluorescence and photoacoustic imaging in living mice. Finally, the rhodol-hybridized probe **45**[24] offered

J. Mex. Chem. Soc. **2026**, *70(1):e2583*
Regular Issue
©2026, Sociedad Química de México
ISSN-e 2594-0317

reversible, ratiometric monitoring of intracellular GSH fluctuations, providing a real-time window into redox regulation. Extending to other RSS, endogenous sulfur dioxide (SO_2), with equilibrates in aqueous medium with HSO_3^- and is generated enzymatically from sulfur-containing amino acids in mitochondria, plays key roles in inflammation, vascular regulation, and sulfur homeostasis. To monitor its biological activity, two indolium-based hemicyanine probes, **46** and **47**,[68] were developed with optimized structural and lipophilic properties for efficient SO_2 detection. The introduction of hydroxyl groups enhanced their fluorescence response toward HSO_3^-, yielding rapid kinetics, low detection limits, and excellent aqueous performance. Notably, the more lipophilic probe **47** exhibited superior mitochondrial targeting and faster response, enabling sensitive imaging of endogenous SO_2 in living systems. Representative chemical structures of sulfur-responsive hemicyanine probes are summarized in Fig. 5.

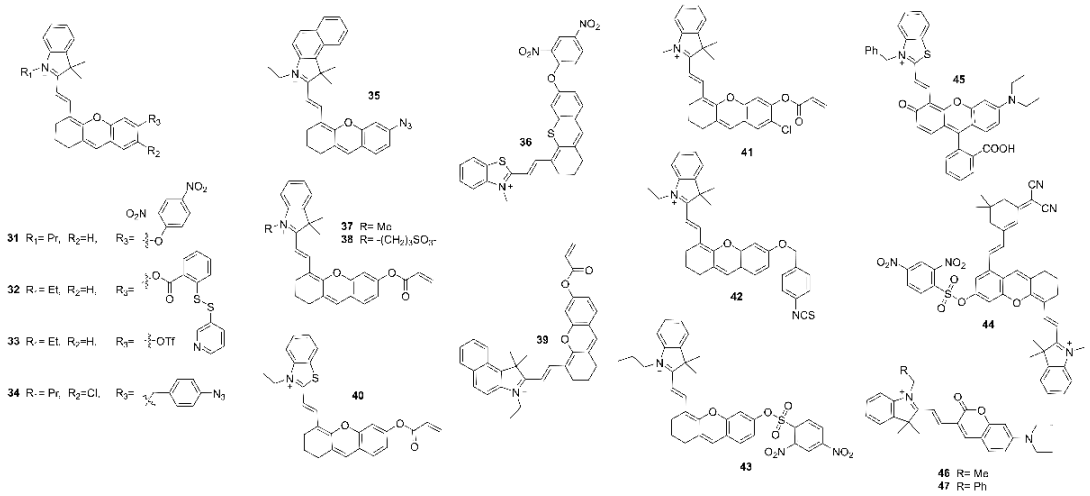

Fig. 5. Hemicyanine-based sensors for RSS.

pH and polarity sensing

Intracellular pH and polarity are fundamental microenvironmental parameters governing enzyme activity, organelle function, and disease progression.[69] The tunable electronic structure of hemicyanine dyes has enabled the creation of a broad family of NIR fluorescent probes for monitoring these factors with high sensitivity and biocompatibility. Several ratiometric pH-responsive systems, such as probes **48**-**52**,[69,70] exploit protonation–deprotonation equilibria to generate pronounced emission shifts and allow precise *in vivo* imaging of acidosis and physiological pH fluctuations. Organelle-targetable probes such as **53**[71] and **54**[72] localize selectively to lysosomes, providing robust platforms for visualizing pH variations during autophagy and drug-induced stress with improved photostability and large Stokes shifts, while probe **55** enables reversible mitochondrial pH sensing.[73] The pyrimidine-fused probe **56**,[74] prepared through a barbiturate-mediated debenzoindolation route, further extends this concept, exhibiting strong NIR fluorescence and excellent spectral sensitivity to environmental pH via deprotonation of the uracil N–H bond. Probes **57** and **58** were designed with enhanced water solubility, high sensitivity, and broad operational range (pH 4.5–10.7), displaying a 30-fold turn-on fluorescence and clear colorimetric change suitable for live-cell pH imaging.[75] Beyond acidity, the ratiometric probe **59** quantifies mitochondrial polarity changes and has revealed decreased polarity during mitophagy for the first time.[76] Collectively, these hemicyanine-based NIR probes for pH and polarity sensing offer powerful molecular tools for dissecting subcellular microenvironment dynamics and their roles in health and disease. Representative chemical structures of pH and polarity sensing hemicyanine probes are summarized in Fig. 6.

http://dx.doi.org/10.29356/jmcs.v70i1.2583

J. Mex. Chem. Soc. **2026**, *70(1):e2583*
Regular Issue
©2026, Sociedad Química de México
ISSN-e 2594-0317

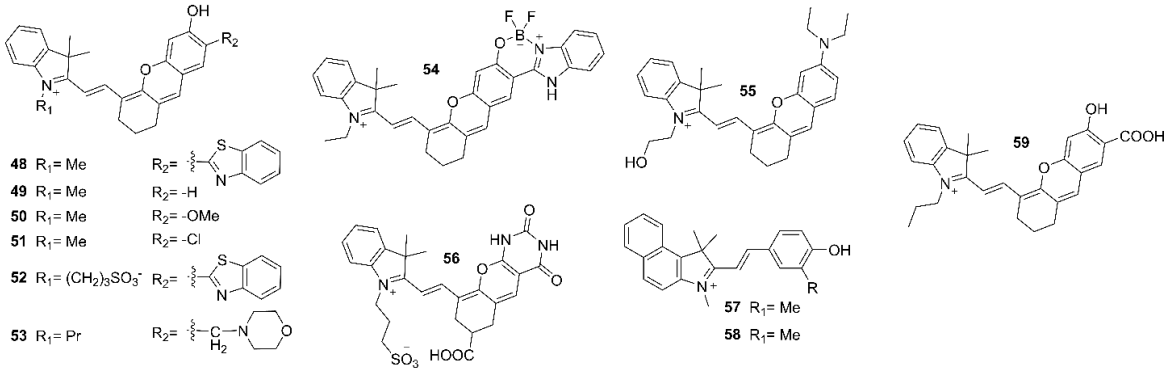

Fig. 6. pH- and polarity-sensing hemicyanine probes.

Viscosity sensing

Viscosity, a critical microenvironmental parameter, influences molecular diffusion, enzyme activity, and cellular metabolism, with abnormal changes linked to diseases such as cancer, diabetes, and neurodegeneration.[77] Hemicyanine-based fluorophores, owing to their strong ICT characteristics and environmental responsiveness, have emerged as powerful molecular tools for real-time viscosity mapping in living systems.[77]

Probe **60** introduced a ratiometric two-photon platform combining dual fluorophores with distinct viscosity sensitivities, enabling quantitative determination of mitochondrial viscosity in living cells and tissues.[78] The NIR probe **61**,[79] incorporating multiple rotatable moieties achieved a 100-fold fluorescence enhancement and was successfully applied to visualize mitochondrial viscosity in inflammatory models. Expanding on this, probe **62** provided deep-red emission and high tissue penetration, allowing, for the first time, *in vivo* visualization of mitochondrial viscosity alterations in fatty liver and tumor-bearing mice.[80]

Further structural refinement produced dual-rotor systems such as probe **63**[81] and probe **64**,[82] which offered superior sensitivity, high signal-to-background ratios, and reliable ratiometric response across cellular and tissue depths up to 130 μm. Meanwhile, the two-photon probe **65**[83] exhibited a 22-fold fluorescence enhancement and enabled dynamic tracking of mitochondrial viscosity fluctuations in living cells, zebrafish, and mice.

To improve solubility and biocompatibility, probe **66**[84] was developed as a hydrophilic benzothiazolium salt derivative capable of detecting viscosity variations between normal and drug-treated mitochondria with a 35-fold fluorescence increase. Similarly, probe **67**,[85] featuring a triphenylamine-functionalized benzothiazole structure, achieved a 94-fold intensity enhancement independent of mitochondrial membrane potential, offering a robust tool for mitochondrial viscosity mapping. The NIR probe **68**,[86] designed with a quinoline acceptor and TICT mechanism, allowed precise visualization of viscosity dynamics during mitophagy, cirrhosis, and starvation-induced stress in cellular and animal models. Finally, the lifetime-based probe **69**[87] provided a quantitative relationship between fluorescence lifetime and viscosity, facilitating highly sensitive monitoring of mitochondrial rheology under diverse biological conditions.

Expanding this toolkit, probe **70**[88] offered rapid mitochondrial accumulation, high photostability, and differentiation between normal and drug-perturbed mitochondria, while probe **71**[89] linked naphthalimide and benzo[e]indolium units to visualize viscosity elevations under inflammation and hyperglycemia.

Two-photon probe **72**[90] utilized a donor–acceptor architecture to monitor mitochondrial viscosity changes during apoptosis with fluorescence lifetime imaging. A systematic series of probes **73**–**78**[91] revealed how structural modification modulates organelle targeting, with some derivatives selective for lysosomal viscosity and others for mitochondria. Similarly, probe **79**[92] integrated a benzo[e]indole–azonia scaffold for simultaneous viscosity detection in mitochondria and lysosomes, achieving a 16-fold signal enhancement and discriminating between cancerous and normal cells. Targeted designs such as probe **80**[93] provided viscosity imaging in biotin receptor–positive cancer cells, while probes **81** and **82**[94] enabled real-time monitoring of nucleolar and chromosomal condensation across cell cycles.

http://dx.doi.org/10.29356/jmcs.v70i1.2583

J. Mex. Chem. Soc. **2026**, *70(1):e2583*
Regular Issue
©2026, Sociedad Química de México
ISSN-e 2594-0317

Extending into advanced imaging regimes, the NIR-II emissive probe **83**[95] represented the first viscosity-activated system beyond 1000 nm, facilitating *in vivo* tracking of liver injury with 31-fold enhancement and high environmental stability. Finally, multifunctional probes **84**[96] and **85**[97] combined viscosity sensing with $ONOO^-$ detection, enabling dual-channel imaging of mitochondrial and hepatic injury during oxidative stress and drug-induced hepatotoxicity.

Building on these advancements, next-generation hemicyanine-based probes have expanded beyond single-parameter detection to simultaneously visualize viscosity and reactive species, providing deeper insight into disease mechanisms. The dual-responsive probe **86**[98] enabled simultaneous monitoring of mitochondrial viscosity and hydrogen peroxide levels via two-photon fluorescence channels, allowing ratiometric imaging in living cells, zebrafish, and Drosophila models of Parkinson's disease. Similarly, probe **87**[99] revealed the interplay between mitochondrial viscosity and H_2S levels in Parkinson's disease, demonstrating that reduced H_2S correlated with increased mitochondrial viscosity, highlighting the molecule's protective role. A NIR probe **88**[100] further extended this approach to Alzheimer's disease, achieving the first *in vivo* imaging of both mitochondrial viscosity and H_2O_2 in rat brains, correlating oxidative stress with increased microviscosity.

Expanding the multimodal strategy, probe **89**[101] provided distinct red and green fluorescence channels for concurrent visualization of viscosity and H_2S, enabling studies on their cross-talk in mitochondrial dysfunction associated with Alzheimer's disease. Likewise, probe **90**[103] and probe **91**[104] offered dual detection of viscosity and SO_2 derivatives using ratiometric two-photon imaging, allowing quantitative mapping of mitochondrial microenvironments in living cells and zebrafish. Notably, probe **92**[104] introduced a fast-responding ratiometric platform for SO_2 detection, demonstrating that increased intracellular viscosity can promote SO_2 accumulation, thereby linking biophysical and chemical stress pathways in cells and mouse models.

Collectively, these viscosity-activated hemicyanine probes (Fig. 7) exemplify the structural versatility and photophysical adaptability of this scaffold for probing subcellular viscosity changes and elucidating their roles in disease-associated biophysical processes.

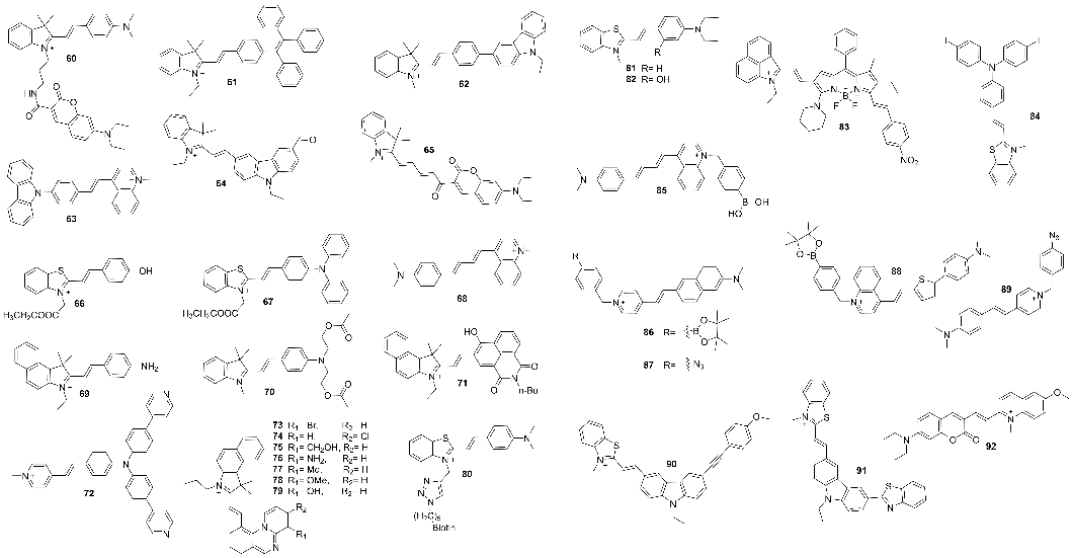

Fig. 7. Viscosity sensing hemicyanine probes.

Metal-ion sensing

Metal ions play pivotal roles in maintaining cellular homeostasis, enzymatic catalysis, and signaling, and their dysregulation is often associated with disease. Hemicyanine-derived NIR probes have proven highly effective for the selective detection and imaging of biologically relevant metal ions owing to their strong ICT character, low background interference, and deep-tissue imaging capability. The mitochondria-targeted probe

http://dx.doi.org/10.29356/jmcs.v70i1.2583

J. Mex. Chem. Soc. **2026**, *70(1):e2583*
Regular Issue
©2026, Sociedad Química de México
ISSN-e 2594-0317

93[105] enables sensitive Cu^{+} detection (LOD = 14 nM) and real-time mapping of mitochondrial copper in live mice, also serving as a non-invasive platform to assess chelation therapy efficacy. A complementary Cu^{2+}-responsive system, probe **94**,[106] utilizes a 2-picolinic ester hydrolysis mechanism to achieve excellent selectivity and a 29 nM detection limit, enabling high-contrast imaging of copper distribution in cells and tissues.

For toxic metal monitoring, probe **95**[107] exploits Hg^{2+}-induced thioacetal deprotection, providing a selective NIR fluorescence "turn-on" response (LOD = 300 nM) and compatibility for both solution and paper-based "naked-eye" detection, as well as live-cell imaging. Expanding into essential ion sensing, probe **96**[108] integrates a BAPTA chelator with a dihydroxanthene–hemicyanine core, offering the first NIR ratiometric fluorescence readout for intracellular Ca^{2+} ($K_d \approx 8$ μM), suitable for quantitative live-cell imaging. Finally, probes **97** and **98** incorporate dipicolylamine recognition motifs for Zn^{2+} detection;[109] notably, probe **97** demonstrates superior selectivity and sensitivity (LOD = 0.5 nM) with strong cellular permeability, whereas probe **98**, featuring a pyrazine-modified dipicolylamine unit, shows limited Zn^{2+} responsiveness. Representative chemical structures of metal ion-sensing hemicyanine probes are summarized in Fig. 8.

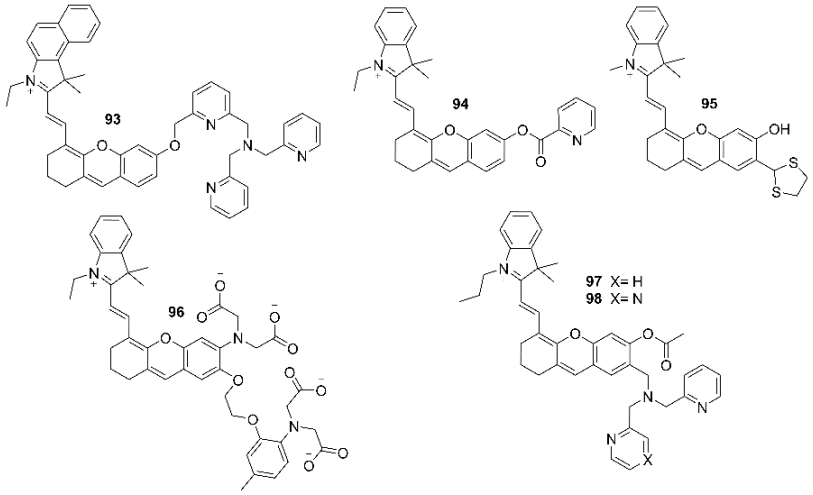

Fig. 8. Metal ion-sensing hemicyanine probes.

Bioconjugation strategies

A defining advantage of hemicyanine dyes is their structural adaptability for bioconjugation, enabling selective targeting, molecular tracking, and bioresponsive activation. Introduction of reactive handles such as carboxyl, maleimide, azide, or alkyne groups permits conjugation via amide coupling, click chemistry, or thiol–ene addition.[3,13,14,22,110–112] Covalent linkage to peptides, antibodies, or aptamers yields probes that preserve biological recognition while providing NIR optical readouts. [3,13,14,22,110–112]

Carboxyl-functionalized hemicyanines exemplify how structural modification enhances both fluorescence control and bioconjugation potential. The Changsha series **99** introduced a carboxylic-acid-regulated spirocyclization mechanism that enables reversible fluorescence ON–OFF switching, producing bright, photostable NIR fluorophores well-suited for developing responsive sensors and offering promising opportunities for bioconjugation.[113] Moreover, probe **100**, functionalized with a carboxylic acid group, was successfully conjugated to the antibody Panitumumab **100-Pan**, showing excellent responsiveness to monoclonal antibody uptake and internalization.[22]

Hemicyanines bearing azido groups for click chemistry provide further flexibility for constructing activatable, biomarker-specific probes. An azido-functionalized NIR-II probe **101** was modified with PEG chains to improve water solubility and subsequently conjugated to a peptide sequence (acetylvaline–citrulline; Ac–Val–Cit) targeting the cancer biomarker cathepsin B, yielding probe **101-CathB**. [14] This construct

J. Mex. Chem. Soc. **2026**, *70(1):e2583*
Regular Issue
©2026, Sociedad Química de México
ISSN-e 2594-0317

enabled high-contrast lung imaging in haired mouse models without the need for shaving, highlighting the suitability of azide-bearing hemicyanines for deep-tissue imaging.

Advancing to more sophisticated bioorthogonal systems, *trans*-cyclooctane (TCO)-functionalized hemicyanines have been integrated into bioorthogonal click platforms for precise and activatable imaging. In this context, probe **102**[111] was designed following a dual-locked enzyme-activatable bioorthogonal fluorescence strategy, in which the TCO-protected hemicyanine reacts selectively with a tetrazine derivative whose reactivity is unmasked only in senescent cancer cells **102-DHP**. This dual-enzyme gating ensures fluorescence activation exclusively within targeted pathological contexts, enabling noninvasive visualization of senescent cancer cells *in vivo*. Representative chemical structures of bioconjugated hemicyanine probes and their reactions are summarized in Scheme 2.

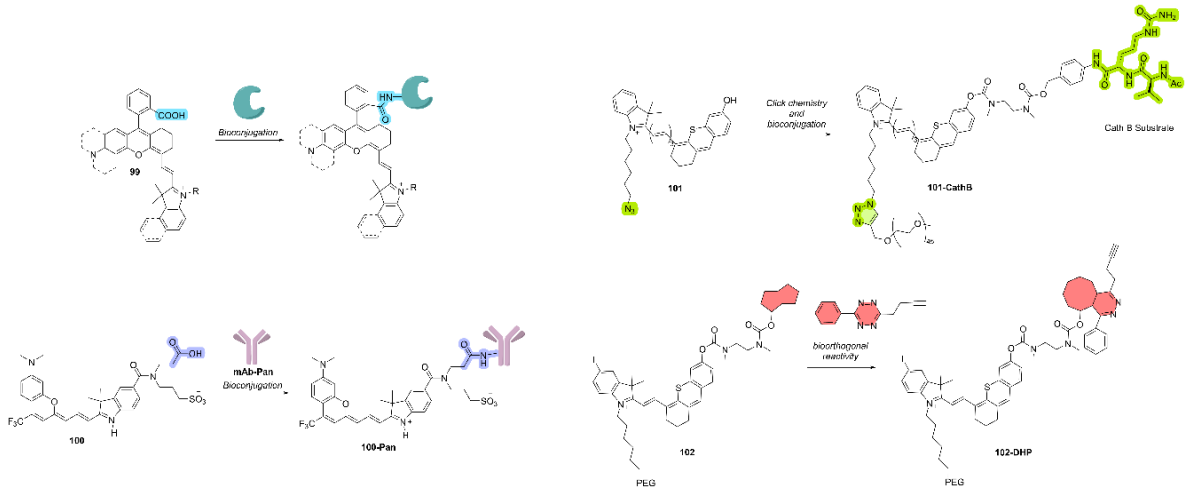

Scheme 2. Bioconjugation strategies with hemicyanine probes.

Modular scaffolds now support enzyme- or redox-activatable groups, including the dual-locked probes **103**[112] and **104**[110] (Fig. 9), which activate fluorescence sequentially through biological triggers.

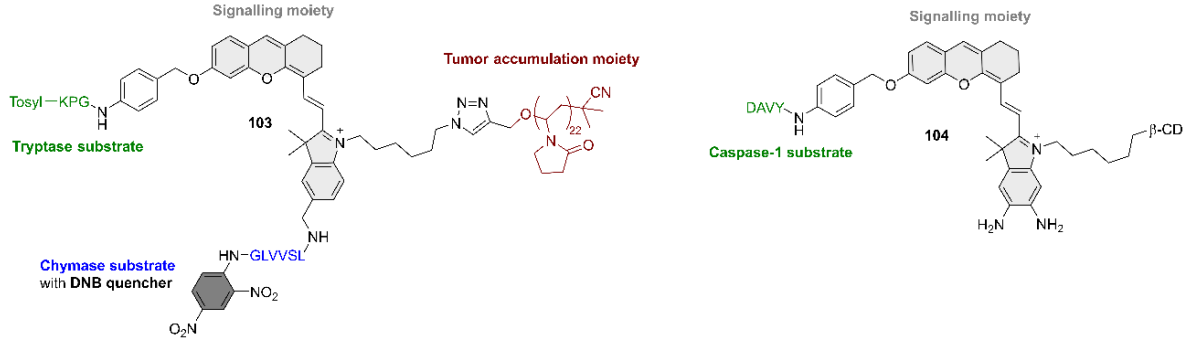

Fig. 9. Dual dual-locked probes.

These studies highlight how hemicyanine scaffolds, through rational incorporation of bioconjugation handles, carboxyl groups for functionalization, azides for click-based modular assembly, and TCOs for precision bioorthogonal activation, serve as highly versatile molecular platforms for building next-generation, targeted, and activatable probes across NIR-I and NIR-II imaging modalities.

http://dx.doi.org/10.29356/jmcs.v70i1.2583

J. Mex. Chem. Soc. **2026**, *70(1):e2583*
Regular Issue
©2026, Sociedad Química de México
ISSN-e 2594-0317

Medicinal chemistry applications

Therapeutic potential

Hemicyanine derivatives have evolved beyond diagnostic agents to emerge as bioactive scaffolds with significant therapeutic potential, particularly in photodynamic and photothermal therapy. Their extended π-conjugation, efficient NIR absorption, and photostable excited states permit deep-tissue activation and localized cytotoxicity with minimal systemic damage. [3,13,19,30,37,38,64]

Biological activities

Hemicyanine dyes possess intrinsic biological activity stemming from their delocalized π-systems, cationic charge, and environment-sensitive electronic structure. Beyond their photophysical advantages, several hemicyanine derivatives exhibit measurable cytotoxic, redox-modulating, and enzyme-interacting properties. The electrophilic character of some analogues enables covalent modification of thiols and redox-active proteins, inducing programmed cell death or redox imbalance. A recent study [114] revealed hemicyanine probe **105** (Fig. 10) as a potent paraptosis inducer, producing endoplasmic reticulum (ER) swelling, mitochondrial enlargement, and superoxide accumulation independent of caspase pathways. Chemoproteomic profiling uncovered Sec23A and GDP-dissociation inhibitor-1 as covalent targets, underscoring hemicyanines' potential as mechanistic probes and therapeutic leads in apoptosis-resistant diseases.

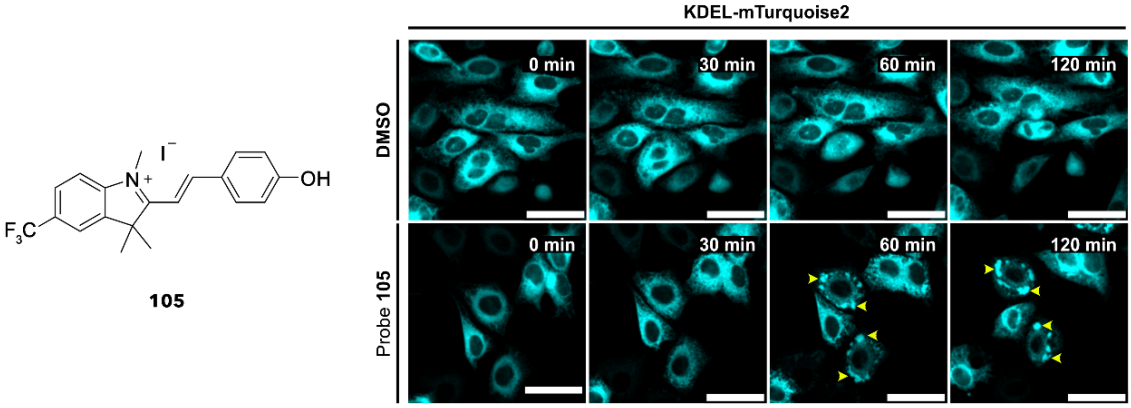

Fig. 10. Hemicyanine probe 105 and paraptosis induction in HeLa cell line transfected with an mTurquoise-KDEL plasmid. Reproduced with permission from Ref. [114] Copyright (2025) American Chemical Society.

Photodynamic therapy

The strong NIR absorption, high singlet oxygen yield, and photostability of hemicyanine derivatives make them ideal photosensitizers for photodynamic therapy. Their donor–π–acceptor (D–π–A) architectures facilitate efficient intersystem crossing and triplet-state formation, generating ROS upon light activation. pH-activatable photosensitizers (e.g., probe **10**) selectively produce singlet oxygen in acidic tumor microenvironments, achieving localized cytotoxicity under 660 nm irradiation.[38] Targeted mitochondrial probes integrate imaging and phototherapeutic capabilities, enabling fluorescence-guided photodynamic ablation with minimal collateral damage. Through rational molecular design, rigid linkers, heavy-atom substitution, and conjugation length optimization, hemicyanine-based photothermal agents achieve high quantum efficiency and deep-tissue efficacy.

Drug delivery and theranostic approaches

Functionalized hemicyanine scaffolds offer dual imaging and therapeutic capabilities—defining hallmarks of theranostics. Conjugation to targeting ligands (peptides, antibodies, or aptamers) enhances selective accumulation in diseased tissues. Bioorthogonal and click-chemistry modifications (e.g., azido or TCO

J. Mex. Chem. Soc. **2026**, *70(1):e2583*
Regular Issue
©2026, Sociedad Química de México
ISSN-e 2594-0317

handles) enable activatable systems responsive to specific enzymatic or redox triggers. For instance, the TCO–hemicyanine system **102** remains non-emissive until dual-enzyme activation unmasks fluorescence selectively in senescent cancer cells, illustrating dual-locked bioorthogonal activation.[111] Additionally, antibody–dye conjugates such as **100–Pan** exploit monoclonal antibody specificity to achieve targeted tumor imaging and therapy. [22] These modular designs integrate delivery precision, diagnostic readouts, and light-triggered therapeutic response in a single platform.

Hemicyanine-based nanoparticles

Nanoparticle formulations significantly enhance hemicyanine performance by improving solubility, stability, and biodistribution. Hemicyanine-based nanoparticles (HCy–NPs) embed dyes in polymeric, lipidic, or silica matrices, preserving fluorescence while preventing aggregation-induced quenching.[31,52] Encapsulation facilitates passive tumor targeting through the enhanced permeability and retention (EPR) effect and enables co-delivery of therapeutic cargos.[31,52] Several nanoliposome-encapsulated probes (e.g., probe **29**) provide dual imaging and therapeutic function, combining NIR fluorescence and photoacoustic modalities for real-time monitoring. [52] The tunable surface chemistry of these nanoparticles also supports stimuli-responsive release, redox activation, and pH-triggered disassembly, advancing precision nanotheranostics.

Theranostic applications

Hemicyanine derivatives are at the forefront of integrated diagnosis and therapy.[115] Dual-modal systems combine fluorescence and photoacoustic imaging with photothermal and photothermal activity.[50,67] Representative multifunctional probes (e.g., **41**, **44**, **85**)[64,67,97] couple analyte responsiveness—toward ROS, RNS, or viscosity—with light-induced cytotoxicity. These agents allow real-time imaging of therapeutic response, bridging molecular diagnostics with treatment feedback loops.[115] NIR-II-active hemicyanine conjugates further extend imaging penetration depth, while mitochondria-targeted variants enable organelle-level monitoring of therapeutic mechanisms. Collectively, these advances establish hemicyanine platforms as versatile agents for image-guided, multimodal, and responsive therapy.

NIR-II dyes for deep-tissue diagnosis

Recent progress has pushed hemicyanine emission beyond 900 nm into the NIR-II region, improving spatial resolution and reducing tissue scattering. NIR-II hemicyanines achieve deep-tissue imaging with superior signal-to-noise ratios, particularly for tumor and vascular visualization (Fig. 11).[13,14,19,95] Structural innovations include benz[e]indolium or phosphinate acceptors, silicon and sulfur heteroatoms, and rigidified π-bridges. Probe **101** exemplifies this trend: an azido-functionalized NIR-II dye conjugated to a cathepsin B-targeting peptide that enabled non-invasive lung imaging in mice without depilation.[14] These systems represent a major advance in deep-tissue diagnostics, uniting biocompatibility, high photostability, and minimal background interference.

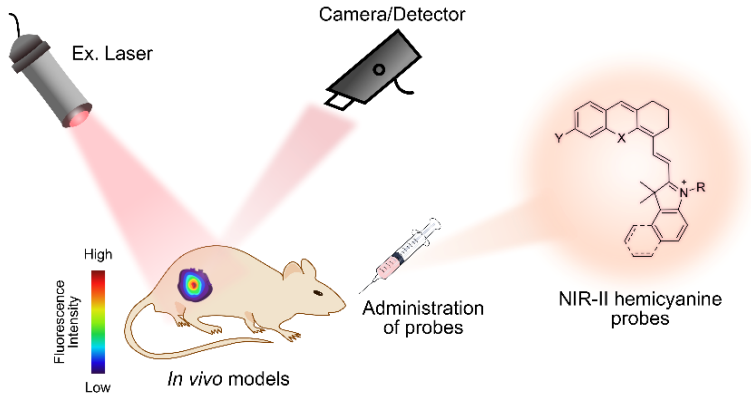

Fig. 11. Representation of *in vivo* NIR-II imaging with hemicyanine probes.

J. Mex. Chem. Soc. **2026**, *70(1):e2583*
Regular Issue
©2026, Sociedad Química de México
ISSN-e 2594-0317

Structure–activity relationships

The photophysical and biological performance of hemicyanines is governed by donor–acceptor modulation and substituent effects:

- *Stronger donors* (julolidine, dialkylamino) and stronger acceptors (indolium, benzothiazolium, quinolinium) red-shift absorption and emission.
- *Heteroatom substitution* (Si, P, S) and bridge rigidification suppress nonradiative decay and enhance photostability.
- *Electron-withdrawing groups* (cyano, nitro, sulfonate) favor photoacoustic and non-fluorescent signal generation.
- *Hybrid architectures* (BODIPY–, xanthene–, rhodol–hemicyanines) achieve balanced fluorescence brightness and tunable emission.

These correlations inform rational probe design, linking structural variation to spectral position, quantum yield, and biological targeting efficiency.

Challenges and limitations

Despite remarkable progress, several limitations constrain hemicyanine applications:

- Photobleaching and oxidation under prolonged irradiation, especially for long-chain polymethines.
- Aggregation and solubility issues in aqueous media, affecting brightness and reproducibility.
- Off-target localization and non-specific binding, owing to cationic charge and lipophilicity.
- Complex synthetic routes for heteroatom and NIR-II analogues limit scalability.

An incomplete understanding of pharmacokinetics and *in vivo* metabolism hinders clinical translation. Addressing these challenges will require stabilizing substituents, controlled nano delivery systems, and detailed toxicological evaluation.

Future perspectives

The next generation of hemicyanine systems is expected to integrate machine-learning-guided molecular design, bioorthogonal activation, and multi-modal imaging. A rational combination of computational photophysics and high-throughput screening will accelerate the discovery of red-shifted, high-quantum-yield scaffolds. Emerging NIR-II-active, activatable, and enzyme-responsive systems promise enhanced diagnostic precision. Incorporation into smart nanoparticles and hybrid nanocomposites will enable synergistic therapy, integrating chemo-, photo-, and immune-modulation. The growing interface between chemistry, nanomedicine, and bioengineering positions hemicyanines as key molecular platforms for the next era of personalized, image-guided therapeutics.

Conclusions

Hemicyanine chromophores, once spectroscopic curiosities, now constitute a cornerstone of biomedical imaging and phototherapy. Their modular D–π–A architecture affords precise control over spectral and functional properties, enabling tailored probes for specific biological contexts. Through advances in molecular engineering, nanoparticle formulation, and conjugation chemistry, hemicyanines have evolved into multifunctional theranostic systems capable of deep-tissue imaging, analyte detection, and targeted treatment. Continued innovation addressing photostability, selectivity, and biocompatibility will consolidate their role in next-generation diagnostic and therapeutic technologies.

http://dx.doi.org/10.29356/jmcs.v70i1.2583

J. Mex. Chem. Soc. **2026**, *70(1):e2583*
Regular Issue
©2026, Sociedad Química de México
ISSN-e 2594-0317

Acknowledgements

We dedicate this review to Prof. Gabriel Cuevas (IQ-UNAM) on the occasion his receiving the Premio Nacional de Química "Andrés Manuel del Río". P. R.-F. acknowledges funding from University of Zurich. J. F. T.-F. acknowledges funding from SECIHTI.

References

1. Jędrzejewska, B.; Kabatc, J.; Pietrzak, M.; Pączkowski, J. *Dyes Pigm.* **2003**, *58*, 47–58. DOI: https://doi.org/10.1016/S0143-7208(03)00035-4.
2. Shindy, H. A. *Dyes Pigm.* **2017**, *145*, 505–513. DOI: https://doi.org/10.1016/j.dyepig.2017.06.029.
3. Li, H.; Kim, H.; Xu, F.; Han, J.; Yao, Q.; Wang, J.; Pu, K.; Peng, X.; Yoon, J. *Chem. Soc. Rev.* **2022**, *51*, 1795–1835. DOI: https://doi.org/10.1039/D1CS00307K.
4. Luo, P.; Wang, M.; Liu, W.; Liu, L.; Xu, P. *Molecules.* **2022**, *27*, 7750. DOI: https://doi.org/10.3390/molecules27227750.
5. Muhammad, S.; Ahmad, H.; Yan, Y.; Chen, X.; Muhammad, S.; Maridevaru, M. C.; Roy, S.; Wang, Z.; Zhang, Y.; Guo, B. *Coord. Chem. Rev.* **2025**, *534*, 216602. DOI: https://doi.org/10.1016/j.ccr.2025.216602.
6. Feng, D.; Guo, L.; Zhao, Y.; Yuan, F.; Ning, L.; Guo, Y.; Zhang, J. *Anal. Chem.* **2025**, *97*, 4041–4048. DOI: https://doi.org/10.1021/acs.analchem.4c05680.
7. Kimura, Y.; Momotake, A.; Takahashi, N.; Kasai, H.; Arai, T. *Chem. Lett.* **2012**, *41*, 528–530. DOI: https://doi.org/10.1246/cl.2012.528.
8. Fromherz, P. *J. Phys. Chem.* **1995**, *99*, 7188–7192. DOI: https://doi.org/10.1021/j100018a061.
9. Zeena, S.; Thomas, K. G. *J. Am. Chem. Soc.* **2001**, *123*, 7859–7865. DOI: https://doi.org/10.1021/ja010199v.
10. Shim, T.; Lee, M. H.; Kim, D.; Ouchi, Y. *J. Phys. Chem. B.* **2008**, *112*, 1906–1912. DOI: https://doi.org/10.1021/jp076757v.
11. Metsov, S.; Dudev, T.; Koleva, V. *J. Mol. Struct.* **1995**, *350*, 241–246. DOI: https://doi.org/10.1016/0022-2860(94)08477-Y.
12. Han, K.; Lu, X.; Xu, J.; Zhou, G.; Ma, S.; Wang, W.; Cai, Z.; Zhou, J. *J. Phys. Appl. Phys.* **1997**, *30*, 2923–2927. DOI: https://doi.org/10.1088/0022-3727/30/21/003.
13. Guo, J.; Zhu, Y.; Qu, Y.; Zhang, L.; Fang, M.; Xu, Z.; Wang, T.; Qin, Y.; Xu, Y.; Li, Y.; Chen, Y.; Fu, H.; Liu, X.; Liu, Y.; Liu, C.; Gao, Y.; Cui, M.; Zhou, K. *J. Med. Chem.* **2024**, *67*, 16820–16834. DOI: https://doi.org/10.1021/acs.jmedchem.4c01662.
14. Yang, H.; Li, D.; Wu, J.; Pu, K. *J. Am. Chem. Soc.* **2025**, *147*, 30794–30802. DOI: https://doi.org/10.1021/jacs.5c06682.
15. East, A. K.; Lee, M. C.; Smaga, L. P.; Jiang, C.; Mallojjala, S. C.; Hirschi, J. S.; Chan, J. *Org. Lett.* **2022**, *24*, 8509–8513. DOI: https://doi.org/10.1021/acs.orglett.2c03382.
16. Yuan, L.; Lin, W.; Zhao, S.; Gao, W.; Chen, B.; He, L.; Zhu, S. *J. Am. Chem. Soc.* **2012**, *134*, 13510–13523. DOI: https://doi.org/10.1021/ja305802v.
17. Luo, S.; Zhang, E.; Su, Y.; Cheng, T.; Shi, C. *Biomaterials.* **2011**, *32*, 7127–7138. DOI: https://doi.org/10.1016/j.biomaterials.2011.06.024.
18. Khalid, M.; Lodhi, H. M.; Khan, M. U.; Imran, M. *RSC Adv.* **2021**, *11*, 14237–14250. DOI: https://doi.org/10.1039/D1RA00876E.
19. Cao, W.; Zhu, Y.; Wu, F.; Tian, Y.; Chen, Z.; Xu, W.; Liu, S.; Liu, T.; Xiong, H. *Small.* **2022**, *18*, 2204851. DOI: https://doi.org/10.1002/smll.202204851.

J. Mex. Chem. Soc. **2026**, *70(1):e2583*
Regular Issue
©2026, Sociedad Química de México
ISSN-e 2594-0317

20. Gardner, S. H.; Brady, C. J.; Keeton, C.; Yadav, A. K.; Mallojjala, S. C.; Lucero, M. Y.; Su, S.; Yu, Z.; Hirschi, J. S.; Mirica, L. M.; Chan, J. *Angew. Chem. Int. Ed.* **2021**, *60*, 18860–18866. DOI: https://doi.org/10.1002/anie.202105905.
21. Richard, J.-A.; Massonneau, M.; Renard, P.-Y.; Romieu, A. *Org. Lett.* **2008**, *10*, 4175–4178. DOI: https://doi.org/10.1021/ol801582w.
22. Caldwell, D. R.; Usama, S. M.; Schnermann, M. J. *Org. Lett.* **2021**, *23*, 8857–8861. DOI: https://doi.org/10.1021/acs.orglett.1c03367.
23. Wang, R.; Chen, J.; Gao, J.; Chen, J.-A.; Xu, G.; Zhu, T.; Gu, X.; Guo, Z.; Zhu, W.-H.; Zhao, C. *Chem. Sci.* **2019**, *10*, 7222–7227. DOI: https://doi.org/10.1039/C9SC02093D.
24. Ren, M.; Wang, L.; Lv, X.; Sun, Y.; Chen, H.; Zhang, K.; Wu, Q.; Bai, Y.; Guo, W. *The Analyst.* **2019**, *144*, 7457–7462. DOI: https://doi.org/10.1039/C9AN01852B.
25. Krieg, R.; Eitner, A.; Günther, W.; Halbhuber, K.-J. *Biotech. Histochem.* **2007**, *82*, 235–262. DOI: https://doi.org/10.1080/10520290701714013.
26. Kuila, S.; Miranda-Salinas, H.; Eng, J.; Li, C.; Bryce, M. R.; Penfold, T. J.; Monkman, A. P. *Nat. Commun.* **2024**, *15*, 9611. DOI: https://doi.org/10.1038/s41467-024-53740-1.
27. Cao, X.; Tolbert, R. W.; McHale, J. L.; Edwards, W. D. *J. Phys. Chem. A.* **1998**, *102*, 2739–2748. DOI: https://doi.org/10.1021/jp972190e.
28. Zhang, X.; Ma, X.; Zhang, B.; Yang, D.; Bai, R.; Gao, Y.; Sun, H.; Tang, Y.; Shi, L. *J. Phys. Chem. B.* **2024**, *128*, 3910–3918. DOI: https://doi.org/10.1021/acs.jpcb.4c00161.
29. Kim, J.; Lee, M. *J. Phys. Chem. A.* **1999**, *103*, 3378–3382. DOI: https://doi.org/10.1021/jp984167e.
30. Zeng, Z.; Liew, S. S.; Wei, X.; Pu, K. *Angew. Chem. Int. Ed.* **2021**, *60*, 26454–26475. DOI: https://doi.org/10.1002/anie.202107877.
31. Wang, X.; Ding, Q.; Groleau, R. R.; Wu, L.; Mao, Y.; Che, F.; Kotova, O.; Scanlan, E. M.; Lewis, S. E.; Li, P.; Tang, B.; James, T. D.; Gunnlaugsson, T. *Chem. Rev.* **2024**, *124*, 7106–7164. DOI: https://doi.org/10.1021/acs.chemrev.3c00776.
32. Wu, L.; Liu, J.; Li, P.; Tang, B.; James, T. D. *Chem. Soc. Rev.* **2021**, *50*, 702–734. DOI: https://doi.org/10.1039/D0CS00861C.
33. Wang, L. V.; Yao, J. *Nat. Methods.* **2016**, *13*, 627–638. DOI: https://doi.org/10.1038/nmeth.3925.
34. Weber, J.; Beard, P. C.; Bohndiek, S. E. *Nat. Methods.* **2016**, *13*, 639–650. DOI: https://doi.org/10.1038/nmeth.3929.
35. Huang, B.; Chen, W.; Kuang, Y.-Q.; Liu, W.; Liu, X.-J.; Tang, L.-J.; Jiang, J.-H. *Org. Biol. Chem.* **2017**, *15*, 4383–4389. DOI: https://doi.org/10.1039/C7OB00781G.
36. Cao, H.; Yu, F.; Dou, K.; Wang, R.; Xing, Y.; Luo, X.; Yu, F. *Anal. Chem.* **2024**, *96*, 18574–18583. DOI: https://doi.org/10.1021/acs.analchem.4c05488.
37. Zhang, L.; Yan, K.; Min, S.; Tan, R.; Deng, S.; Deng, Y.; Zhang, H.; Yao, Y.; Liu, Y.; Yang, X.; Xiong, J.; Wang, J.; Gao, T. *J. Phys. Chem. Lett.* **2025**, *16*, 1746–1752. DOI: https://doi.org/10.1021/acs.jpclett.4c03655.
38. Liu, Y.; Li, Y.; Sun, W.; Sun, Z.; Wang, Y.; Lei, S.; Huang, P.; Lin, J. *Anal. Chem.* **2025**, *97*, 3310–3318. DOI: https://doi.org/10.1021/acs.analchem.4c05056.
39. Xie, X.; Yang, X.; Wu, T.; Li, Y.; Li, M.; Tan, Q.; Wang, X.; Tang, B. *Anal. Chem.* **2016**, *88*, 8019–8025. DOI: https://doi.org/10.1021/acs.analchem.6b01256.
40. Wang, S.; Zhang, Y.; Wang, T.-R.; Liu, Y.-J.; Shen, S.-L.; Cao, X.-Q. *Spectrochim. Acta A Mol. Biomol. Spectrosc.* **2022**, *266*, 120435. DOI: https://doi.org/10.1016/j.saa.2021.120435.
41. Xu, F.; Li, H.; Yao, Q.; Fan, J.; Wang, J.; Peng, X. *J. Mater. Chem. B.* **2016**, *4*, 7363–7367. DOI: https://doi.org/10.1039/C6TB02463G.
42. Zhang, J.; Shi, L.; Li, Z.; Li, D.; Tian, X.; Zhang, C. *The Analyst.* **2019**, *144*, 3643–3648. DOI: https://doi.org/10.1039/C9AN00385A.
43. Hao, Y.; Li, Z.; Ding, N.; Tang, X.; Zhang, C. *Spectrochim. Acta A Mol. Biomol. Spectrosc.* **2022**, *268*, 120642. DOI: https://doi.org/10.1016/j.saa.2021.120642.
44. Alouane, A.; Labruère, R.; Le Saux, T.; Schmidt, F.; Jullien, L. *Angew. Chem. Int. Ed.* **2015**, *54*, 7492–7509. DOI: https://doi.org/10.1002/anie.201500088.
45. Ma, J.; Yan, C.; Li, Y.; Duo, H.; Li, Q.; Lu, X.; Guo, Y. *Chem. – Eur. J.* **2019**, *25*, 7168–7176. DOI: https://doi.org/10.1002/chem.201806264.

J. Mex. Chem. Soc. **2026**, *70(1):e2583*
Regular Issue
©2026, Sociedad Química de México
ISSN-e 2594-0317

46. Gao, W.; Ma, Y.; Liu, Y.; Ma, S.; Lin, W. *Sens. Actuators B Chem.* **2021**, *327*, 128884. DOI: https://doi.org/10.1016/j.snb.2020.128884.
47. Qian, X.; Yu, H.; Zhu, W.; Yao, X.; Liu, W.; Yang, S.; Zhou, F.; Liu, Y. *Dyes Pigm.* **2021**, *188*, 109218. DOI: https://doi.org/10.1016/j.dyepig.2021.109218.
48. Zhang, J.; Li, C.; Zhang, R.; Zhang, F.; Liu, W.; Liu, X.; Lee, S. M.-Y.; Zhang, H. *Chem. Commun.* **2016**, *52*, 2679–2682. DOI: https://doi.org/10.1039/C5CC09976E.
49. Wu, L.; Liu, J.; Tian, X.; Groleau, R. R.; Bull, S. D.; Li, P.; Tang, B.; James, T. D. *Chem. Sci.* **2021**, *12*, 3921–3928. DOI: https://doi.org/10.1039/D0SC05937D.
50. Zhang, J.; Zhen, X.; Zeng, J.; Pu, K. *Anal. Chem.* **2018**, *90*, 9301–9307. DOI: https://doi.org/10.1021/acs.analchem.8b01879.
51. Zhou, D.-Y.; Li, Y.; Jiang, W.-L.; Tian, Y.; Fei, J.; Li, C.-Y. *Chem. Commun.* **2018**, *54*, 11590–11593. DOI: https://doi.org/10.1039/C8CC07389A.
52. Zhang, J.; Kan, J.; Sun, Y.; Won, M.; Kim, J. H.; Zhang, W.; Zhou, J.; Qian, Z.; Kim, J. S. *ACS Appl. Bio Mater.* **2021**, *4*, 2080–2088. DOI: https://doi.org/10.1021/acsabm.0c01178.
53. Sonawane, P. M.; Lee, W.; Kim, Y.; Roychaudhury, A.; Bhosale, V. K.; Kim, D.; Park, H.-S.; Kim, C.-H.; Churchill, D. G. *Spectrochim. Acta A Mol. Biomol. Spectrosc.* **2022**, *267*, 120568. DOI: https://doi.org/10.1016/j.saa.2021.120568.
54. Zhang, L.; Zheng, X. E.; Zou, F.; Shang, Y.; Meng, W.; Lai, E.; Xu, Z.; Liu, Y.; Zhao, J. *Sci. Rep.* **2016**, *6*, 18868. DOI: https://doi.org/10.1038/srep18868.
55. Ma, J.; Li, F.; Li, Q.; Li, Y.; Yan, C.; Lu, X.; Guo, Y. *New J. Chem.* **2018**, *42*, 19272–19278. DOI: https://doi.org/10.1039/C8NJ04208J.
56. Zhang, X.; Sun, R.; Duan, G.; Zhou, Z.; Luo, Y.; Li, W.; Zhang, L.; Gu, Y.; Zha, X. *New J. Chem.* **2018**, *42*, 19795–19800. DOI: https://doi.org/10.1039/C8NJ04824J.
57. Park, C. S.; Ha, T. H.; Choi, S.-A.; Nguyen, D. N.; Noh, S.; Kwon, O. S.; Lee, C.-S.; Yoon, H. *Biosens. Bioelectron.* **2017**, *89*, 919–926. DOI: https://doi.org/10.1016/j.bios.2016.09.093.
58. Yao, X.; Liu, W.; Zhu, W.; Tiemuer, A.; Zhou, F.; Yang, S.; Yu, H.; Qian, X.; Liu, Y. *Chem. Commun.* **2020**, *56*, 8111–8114. DOI: https://doi.org/10.1039/D0CC02814B.
59. Su, W.; Huang, L.; Zhu, L.; Lin, W. *Sens. Actuators B Chem.* **2022**, *369*, 132297. DOI: https://doi.org/10.1016/j.snb.2022.132297.
60. Zhang, J.; Wang, J.; Liu, J.; Ning, L.; Zhu, X.; Yu, B.; Liu, X.; Yao, X.; Zhang, H. *Anal. Chem.* **2015**, *87*, 4856–4863. DOI: https://doi.org/10.1021/acs.analchem.5b00377.
61. Qi, S.; Zhu, L.; Wang, X.; Du, J.; Yang, Q.; Li, Y. *RSC Adv.* **2019**, *9*, 41431–41437. DOI: https://doi.org/10.1039/C9RA08555F.
62. Han, C.; Yang, H.; Chen, M.; Su, Q.; Feng, W.; Li, F. *ACS Appl. Mater. Interfaces.* **2015**, *7*, 27968–27975. DOI: https://doi.org/10.1021/acsami.5b10607.
63. Li, Y.; He, X.; Huang, Y.; Xu, L.; Zhao, L.; Li, X.; Sun, Y.; Wang, X.; Ma, P.; Song, D. *Spectrochim. Acta A Mol. Biomol. Spectrosc.* **2020**, *226*, 117544. DOI: https://doi.org/10.1016/j.saa.2019.117544.
64. Savani, S.; Onbasli, K.; Gunduz, H.; Celikbas, E.; Erkısa, M.; Muti, A.; Khan, M.; Sennaroglu, A.; Ulukaya, E.; Yagci Acar, H.; Kolemen, S. *Bioorg. Chem.* **2022**, *122*, 105725. DOI: https://doi.org/10.1016/j.bioorg.2022.105725.
65. Zhang, M.; Wang, S.; Fu, Y.; Meng, M.; Jin, H.; Zhao, W. *Sens. Actuators B Chem.* **2022**, *366*, 132013. DOI: https://doi.org/10.1016/j.snb.2022.132013.
66. Li, L.-L.; He, P.-Y.; Shi, L.; Pan, S.-L.; Li, M.-Y.; Zhou, Q.; Zhang, H.; Wang, N.; Li, K.; Yu, X.-Q. *Anal. Methods.* **2019**, *11*, 821–826. DOI: https://doi.org/10.1039/C8AY02505C.
67. Qin, J.; Tian, H.; Kong, F.; Guo, Y.; Du, W.; Zhang, C.; Gu, H.; Li, Y. *Sens. Actuators B Chem.* **2022**, *371*, 132522. DOI: https://doi.org/10.1016/j.snb.2022.132522.
68. Chao, J.; Wang, Z.; Zhang, T.; Zhang, Y.; Huo, F. *Spectrochim. Acta A Mol. Biomol. Spectrosc.* **2022**, *266*, 120444. DOI: https://doi.org/10.1016/j.saa.2021.120444.
69. Li, Y.; Wang, Y.; Yang, S.; Zhao, Y.; Yuan, L.; Zheng, J.; Yang, R. *Anal. Chem.* **2015**, *87*, 2495–2503. DOI: https://doi.org/10.1021/ac5045498.
70. Wang, B.-L.; Jiang, C.; Li, K.; Liu, Y.-H.; Xie, Y.; Yu, X.-Q. *The Analyst.* **2015**, *140*, 4608–4615. DOI: https://doi.org/10.1039/C5AN00551E.

J. Mex. Chem. Soc. **2026**, *70(1):e2583*
Regular Issue
©2026, Sociedad Química de México
ISSN-e 2594-0317

71. Wan, Q.; Chen, S.; Shi, W.; Li, L.; Ma, H. *Angew. Chem. Int. Ed.* **2014**, *53*, 10916–10920. DOI: https://doi.org/10.1002/anie.201405742.
72. Shi, Y.; Meng, X.; Yang, H.; Song, L.; Liu, S.; Xu, A.; Chen, Z.; Huang, W.; Zhao, Q. *J. Mater. Chem. B.* **2019**, *7*, 3569–3575. DOI: https://doi.org/10.1039/C8TB03353F.
73. Mazi, W.; Yan, Y.; Zhang, Y.; Xia, S.; Wan, S.; Tajiri, M.; Luck, R. L.; Liu, H. *J. Mater. Chem. B.* **2021**, *9*, 857–863. DOI: https://doi.org/10.1039/D0TB02181D.
74. Lee, H.; Berezin, M. Y.; Guo, K.; Kao, J.; Achilefu, S. *Org. Lett.* **2009**, *11*, 29–32. DOI: https://doi.org/10.1021/ol802363x.
75. Li, X.; Yue, Y.; Wen, Y.; Yin, C.; Huo, F. *Dyes Pigm.* **2016**, *134*, 291–296. DOI: https://doi.org/10.1016/j.dyepig.2016.07.033.
76. Li, X.; Li, X.; Ma, H. *Chem. Sci.* **2020**, *11*, 1617–1622. DOI: https://doi.org/10.1039/C9SC05505C.
77. Xiao, H.; Li, P.; Tang, B. *Chem. – Eur. J.* **2021**, *27*, 6880–6898. DOI: https://doi.org/10.1002/chem.202004888.
78. Ren, M.; Zhou, K.; Wang, L.; Liu, K.; Lin, W. *Sens. Actuators B Chem.* **2018**, *262*, 452–459. DOI: https://doi.org/10.1016/j.snb.2018.02.044.
79. Ma, Y.; Zhao, Y.; Guo, R.; Zhu, L.; Lin, W. *J. Mater. Chem. B.* **2018**, *6*, 6212–6216. DOI: https://doi.org/10.1039/C8TB02083C.
80. Yin, J.; Peng, M.; Lin, W. *Anal. Chem.* **2019**, *91*, 8415–8421. DOI: https://doi.org/10.1021/acs.analchem.9b01293.
81. Yang, Y.; He, L.; Lin, W. *J. Photochem. Photobiol. A Chem.* **2020**, *401*, 112789. DOI: https://doi.org/10.1016/j.jphotochem.2020.112789.
82. Liu, F.; Luo, Y.; Xu, M. *Tetrahedron Lett.* **2018**, *59*, 4540–4544. DOI: https://doi.org/10.1016/j.tetlet.2018.11.009.
83. Peng, M.; Yin, J.; Lin, W. *New J. Chem.* **2019**, *43*, 16945–16949. DOI: https://doi.org/10.1039/C9NJ03744F.
84. Wang, H.; Fang, B.; Xiao, L.; Li, D.; Zhou, L.; Kong, L.; Yu, Y.; Li, X.; Wu, Y.; Hu, Z. *Spectrochim. Acta A Mol. Biomol. Spectrosc.* **2018**, *203*, 127–131. DOI: https://doi.org/10.1016/j.saa.2018.05.121.
85. Wang, H.; Zhou, L.; Cai, F.; Shen, X.; Sun, J.; Wei, Y.; Feng, D.; Feng, Z.; He, J. *Chem. Pap.* **2020**, *74*, 1071–1078. DOI: https://doi.org/10.1007/s11696-019-00946-z.
86. Zhang, Y.; Li, Z.; Hu, W.; Liu, Z. *Anal. Chem.* **2019**, *91*, 10302–10309. DOI: https://doi.org/10.1021/acs.analchem.9b02678.
87. Chen, B.; Li, C.; Zhang, J.; Kan, J.; Jiang, T.; Zhou, J.; Ma, H. *Chem. Commun.* **2019**, *55*, 7410–7413. DOI: https://doi.org/10.1039/C9CC03977E.
88. Wang, H.; Cai, F.; Zhou, L.; He, J.; Feng, D.; Wei, Y.; Feng, Z.; Gu, X.; Kajsa, U.; Hu, Z. *New J. Chem.* **2019**, *43*, 8811–8815. DOI: https://doi.org/10.1039/C9NJ01826C.
89. Zhu, L.; Fu, M.; Yin, B.; Wang, L.; Chen, Y.; Zhu, Q. *Dyes Pigm.* **2020**, *172*, 107859. DOI: https://doi.org/10.1016/j.dyepig.2019.107859.
90. Hou, M.-X.; Liu, L.-Y.; Wang, K.-N.; Chao, X.-J.; Liu, R.-X.; Mao, Z.-W. *New J. Chem.* **2020**, *44*, 11342–11348. DOI: https://doi.org/10.1039/D0NJ02108C.
91. Yang, X.-Z.; Xu, B.; Shen, L.; Sun, R.; Xu, Y.-J.; Song, Y.-L.; Ge, J.-F. *Anal. Chem.* **2020**, *92*, 3517–3521. DOI: https://doi.org/10.1021/acs.analchem.0c00054.
92. Wei, Y.-F.; Weng, X.-F.; Sha, X.-L.; Sun, R.; Xu, Y.-J.; Ge, J.-F. *Sens. Actuators B Chem.* **2021**, *326*, 128954. DOI: https://doi.org/10.1016/j.snb.2020.128954.
93. Ren, M.; Xu, Q.; Wang, S.; Liu, L.; Kong, F. *Chem. Commun.* **2020**, *56*, 13351–13354. DOI: https://doi.org/10.1039/D0CC05039C.
94. Wang, K.-N.; Chao, X.-J.; Liu, B.; Zhou, D.-J.; He, L.; Zheng, X.-H.; Cao, Q.; Tan, C.-P.; Zhang, C.; Mao, Z.-W. *Chem. Commun.* **2018**, *54*, 2635–2638. DOI: https://doi.org/10.1039/C8CC00256H.
95. Dou, K.; Huang, W.; Xiang, Y.; Li, S.; Liu, Z. *Anal. Chem.* **2020**, *92*, 4177–4181. DOI: https://doi.org/10.1021/acs.analchem.0c00634.
96. Sun, W.; Shi, Y.-D.; Ding, A.-X.; Tan, Z.-L.; Chen, H.; Liu, R.; Wang, R.; Lu, Z.-L. *Sens. Actuators B Chem.* **2018**, *276*, 238–246. DOI: https://doi.org/10.1016/j.snb.2018.08.045.
97. Deng, Y.; Feng, G. *Anal. Chem.* **2020**, *92*, 14667–14675. DOI: https://doi.org/10.1021/acs.analchem.0c03199.

J. Mex. Chem. Soc. **2026**, *70(1):e2583*
Regular Issue
©2026, Sociedad Química de México
ISSN-e 2594-0317

98. Li, H.; Xin, C.; Zhang, G.; Han, X.; Qin, W.; Zhang, C.; Yu, C.; Jing, S.; Li, L.; Huang, W. *J. Mater. Chem. B.* **2019**, *7*, 4243–4251. DOI: https://doi.org/10.1039/C9TB00576E.
99. Fang, Z.; Su, Z.; Qin, W.; Li, H.; Fang, B.; Du, W.; Wu, Q.; Peng, B.; Li, P.; Yu, H.; Li, L.; Huang, W. *Chin. Chem. Lett.* **2020**, *31*, 2903–2908. DOI: https://doi.org/10.1016/j.cclet.2020.03.063.
100. Li, S.; Wang, P.; Feng, W.; Xiang, Y.; Dou, K.; Liu, Z. *Chem. Commun.* **2020**, *56*, 1050–1053. DOI: https://doi.org/10.1039/C9CC08267K.
101. Li, S.-J.; Li, Y.-F.; Liu, H.-W.; Zhou, D.-Y.; Jiang, W.-L.; Ou-Yang, J.; Li, C.-Y. *Anal. Chem.* **2018**, *90*, 9418–9425. DOI: https://doi.org/10.1021/acs.analchem.8b02068.
102. Fang, G.; Yang, X.; Wang, W.; Feng, Y.; Zhang, W.; Huang, Y.; Sun, C.; Chen, M.; Meng, X. *Sens. Actuators B Chem.* **2019**, *297*, 126777. DOI: https://doi.org/10.1016/j.snb.2019.126777.
103. Sun, C.; Cao, W.; Zhang, W.; Zhang, L.; Feng, Y.; Fang, M.; Xu, G.; Shao, Z.; Yang, X.; Meng, X. *Dyes Pigm.* **2019**, *171*, 107709. DOI: https://doi.org/10.1016/j.dyepig.2019.107709.
104. Ma, T.; Huo, F.; Chao, J.; Li, J.; Yin, C. *Sens. Actuators B Chem.* **2020**, *320*, 128044. DOI: https://doi.org/10.1016/j.snb.2020.128044.
105. Qian, X.; Zhu, W.; Yu, H.; Xu, Y.; Liu, W.; Wang, H.-Y.; Liu, Y. *Dyes Pigm.* **2021**, *194*, 109561. DOI: https://doi.org/10.1016/j.dyepig.2021.109561.
106. Zhang, H.; Feng, L.; Jiang, Y.; Wong, Y.-T.; He, Y.; Zheng, G.; He, J.; Tan, Y.; Sun, H.; Ho, D. *Biosens. Bioelectron.* **2017**, *94*, 24–29. DOI: https://doi.org/10.1016/j.bios.2017.02.037.
107. Wang, Y.; Hou, X.; Li, Z.; Liu, C.; Hu, S.; Li, C.; Xu, Z.; Wang, Y. *Dyes Pigm.* **2020**, *173*, 107951. DOI: https://doi.org/10.1016/j.dyepig.2019.107951.
108. Collot, M.; Ponsot, F.; Klymchenko, A. S. *Chem. Commun.* **2017**, *53*, 6117–6120. DOI: https://doi.org/10.1039/C7CC02418E.
109. Fang, M.; Xia, S.; Bi, J.; Wigstrom, T. P.; Valenzano, L.; Wang, J.; Tanasova, M.; Luck, R. L.; Liu, H. *Molecules.* **2019**, *24*, 1592. DOI: https://doi.org/10.3390/molecules24081592.
110. Hu, Y.; Liu, J.; Xu, M.; Pu, K. *J. Am. Chem. Soc.* **2025**, *147*, 7148–7157. DOI: https://doi.org/10.1021/jacs.5c00506.
111. Wang, X.; Liew, S. S.; Huang, J.; Hu, Y.; Wei, X.; Pu, K. *J. Am. Chem. Soc.* **2024**, *146*, 22689–22698. DOI: https://doi.org/10.1021/jacs.4c07286.
112. Hu, Y.; Yu, J.; Xu, M.; Pu, K. *J. Am. Chem. Soc.* **2024**, *146*, 12656–12663. DOI: https://doi.org/10.1021/jacs.4c02070.
113. Yuan, L.; Lin, W.; Yang, Y.; Chen, H. *J. Am. Chem. Soc.* **2012**, *134*, 1200–1211. DOI: https://doi.org/10.1021/ja209292b.
114. Tamez-Fernández, J. F.; Steven, C. F.; Nguyen, J.; Rivera-Fuentes, P. *J. Am. Chem. Soc.* **2025**, *jacs.5c07109*. DOI: https://doi.org/10.1021/jacs.5c07109.
115. Sharma, A.; Verwilst, P.; Li, M.; Ma, D.; Singh, N.; Yoo, J.; Kim, Y.; Yang, Y.; Zhu, J.-H.; Huang, H.; Hu, X.-L.; He, X.-P.; Zeng, L.; James, T. D.; Peng, X.; Sessler, J. L.; Kim, J. S. *Chem. Rev.* **2024**, *124*, 2699–2804. DOI: https://doi.org/10.1021/acs.chemrev.3c00778.